

NOTICE: This is the accepted author manuscript of the publication

**A High-Resolution In Vivo Atlas of the Human Brain's Serotonin System.**

Beliveau V, Ganz M, Feng L, Ozenne B, Højgaard L, Fisher PM, Svarer C, Greve DN,  
Knudsen GM.

Published in

**J Neurosci. 2017 Jan 4;37(1):120-128.**

**doi: 10.1523/JNEUROSCI.2830-16.2016.**

Direct link to the final version of the article:

<https://doi.org/10.1523/JNEUROSCI.2830-16.2016>

© <2017>. This manuscript version is made available under the CC-BY-NC-ND 4.0 license  
<http://creativecommons.org/licenses/by-nc-nd/4.0/>

# 1 **A high-resolution in vivo atlas of the human brain's serotonin system**

2 Vincent Beliveau<sup>1,2</sup>, Melanie Ganz<sup>1</sup>, Ling Feng<sup>1</sup>, Brice Ozenne<sup>1,3</sup>, Liselotte Højgaard<sup>2,4</sup>, Patrick M.  
3 Fisher<sup>1</sup>, Claus Svarer<sup>1</sup>, Douglas N. Greve<sup>5,6</sup>, Gitte M. Knudsen<sup>1,2,\*</sup>

4  
5 <sup>1</sup>Neurobiology Research Unit and Center for Integrated Molecular Brain Imaging, Rigshospitalet,  
6 DK-2100 Copenhagen, Denmark

7 <sup>2</sup>Faculty of Health and Medical Sciences, Copenhagen University, DK-2100 Copenhagen, Denmark

8 <sup>3</sup>Department of Public Health, Section of Biostatistics, Copenhagen University, DK-2100  
9 Copenhagen, Denmark

10 <sup>4</sup>PET and Cyclotron Unit, Copenhagen University Hospital, Rigshospitalet, DK-2100 Copenhagen,  
11 Denmark

12 <sup>5</sup>Athinoula A. Martinos Center for Biomedical Imaging, Department of Radiology, Massachusetts  
13 General Hospital, Boston, MA 02129, USA

14 <sup>6</sup>Harvard Medical School, Boston, MA 02115, USA

15  
16 \*Corresponding Author

17 Gitte M. Knudsen, MD, DMSc

18 Neurobiology Research Unit

19 Rigshospitalet

20 9 Blegdamsvej, Section 6931

21 DK-2100 Copenhagen, Denmark

22 Phone: +45 3545 6720

23 E-mail: [gmk@nru.dk](mailto:gmk@nru.dk)

24  
25 Pages: 20    Figures: 6    Tables: 2

26 Words:        Abstract: 176        Introduction: 635    Discussion: 1291

## 27 28 **Conflict of interest**

29 V.B., M.G., L.F., P.M.F., C.S. and D.N.G. declare no competing financial interest. G.M.K. has  
30 been an invited lecturer at Pfizer A/S, worked as a consultant and received grants from H. Lundbeck  
31 A/S and is a stock holder of Novo Nordisk/Novozymes. Furthermore, she is on the board of directors  
32 of the BrainPrize and Elsass foundation and the advisory board of the Kristian Jebsen Foundation and  
33 has authored for FADL and served as editor for Elsevier (IJNP). L.H. is chairman of the board of the  
34 Danish National Research Foundation, and on the board of the Science advisory board of the Olav  
35 Thon Foundation and chairman of the Advisory Board of EU Horizon 2020, Health demographic  
36 change and wellbeing.

## 37 38 **Acknowledgement**

39 Collection of data included in the study was supported by the Lundbeck Foundation Center  
40 Cimbi (R90-A7722). V.B. was supported by the Danish Council for Independent Research - Medical  
41 Sciences (4183-00627) and the Research Council of Rigshospitalet (R84-A3300). M.G. was  
42 supported by the Carlsberg foundation (2013-01-0502) and National Institutes of Health  
43 (5R21EB018964-02). L.F. was supported by the European Union's Seventh Framework Programme  
44 (FP7/2007-2013) under grant agreement n° HEALTH-F2-2011-278850 (INMiND). D.N.G. research  
45 was supported by the NIH grant Multimodal Brain Imaging of Serotonin (5R21EB018964-02) and  
46 the MGH grant Shared Instrumentation Grant (S10RR023043). We thank The John and Birthe Meyer  
47 Foundation for providing the PET HRRT scanner.

## 1 **Abstract**

2           The serotonin (5-HT) system modulates many important brain functions and is critically  
3 involved in many neuropsychiatric disorders. We here present a high-resolution multi-dimensional *in*  
4 *vivo* atlas of four of the human brain's 5-HT receptors (5-HT<sub>1A</sub>, 5-HT<sub>1B</sub>, 5-HT<sub>2A</sub>, and 5-HT<sub>4</sub>) as well  
5 as of the 5-HT transporter (5-HTT). The atlas is created from molecular and structural high-resolution  
6 neuroimaging data consisting of Positron Emission Tomography (PET) and Magnetic Resonance  
7 Imaging (MRI) scans, acquired in a total of 210 healthy individuals. Comparison of the regional PET  
8 binding measures with postmortem human brain autoradiography outcomes showed a high  
9 correlation for the five 5-HT targets and this enabled us to transform the atlas to represent protein  
10 densities (pmol/ml). We also assessed the regional association between protein concentration and  
11 mRNA expression in the human brain by comparing the 5-HT density across the atlas to data from  
12 the Allen Human Brain atlas and identified receptor- and transporter specific associations which  
13 inform about the regional relation between the two measures. Together, these data provide  
14 unparalleled insight into the serotonin system of the human brain.

15

## 1 **Significance Statement**

2           We present a high-resolution PET and MR-based human brain atlas of important serotonin  
3 receptors and the transporter. The regional PET-derived binding measures correlate strongly with the  
4 corresponding autoradiography protein levels. The strong correlation enables the transformation of  
5 the PET-derived human brain atlas into a protein density map of the 5-HT system. Next, we compared  
6 the regional receptor/transporter protein densities to mRNA levels, and uncovered unique associations  
7 between protein expression and density at high detail. This new in vivo neuroimaging atlas of the 5-  
8 HT system does not only provide insight in the human brain's regional protein synthesis, transport  
9 and density, but also represents a valuable source of information for the neuroscience community as  
10 a comparative instrument to assess brain disorders.

## 1 **Introduction**

2 Serotonin (5-hydroxytryptamine, 5-HT) is a highly evolutionary conserved monoamine  
3 neurotransmitter that across species modulates multiple psycho-physiological functions. In the human  
4 brain, 5-HT is synthesized within the brainstems' raphe nuclei which have distributed efferent and  
5 afferent projections throughout the brain (Dorocic et al., 2014). The 5-HT system is highly diverse  
6 (Hannon and Hoyer, 2008); based on structural, transductional and operational features its receptors  
7 have been grouped into 7 families of receptors (5-HT<sub>1</sub> to 5-HT<sub>7</sub>), including 14 known subtypes, and  
8 a transporter (5-HTT). Of the 14 receptors, there are 13 distinct G protein-coupled receptors and one  
9 ligand-gated ion channel receptor, the 5-HT<sub>3</sub>. 5-HT is involved in myriad physiological functions  
10 such as cognition (Meneses, 1999), mood and social interaction (Young and Leyton, 2002), sexual  
11 behavior (Waldinger, 2015), feeding behavior (Magalhães et al., 2010), sleep-wake cycle (Portas et  
12 al., 2000) and thermoregulation (Cryan et al., 2000). Disturbances in the 5-HT system are also linked  
13 to many debilitating brain disorders such as major depression, anxiety, and schizophrenia as well as  
14 migraine and neurodegenerative disorders (Oades, 2010). The role of the individual receptors in the  
15 different functions and disorders is, however, only partially known. A prominent example is that even  
16 though the 5-HTT inhibitors (SSRIs) are the most frequently prescribed antidepressant drug class, the  
17 exact involvement of individual 5-HT receptors in mediating its clinical effects is still unclear. To  
18 study the role of the individual receptors in healthy individuals, in patients with brain disorders and  
19 in response to physiological or drug interventions, in vivo molecular brain imaging with positron  
20 emission tomography (PET) in conjunction with an appropriate radiotracer represents the state-of-  
21 the-art approach for quantifying the density and spatial distribution of brain receptors and transporters.

22 Brain atlases play a key role in neuroimaging research. Stereotactic atlases of magnetic  
23 resonance imaging (MRI) brain morphology such as the Talairach (Talairach and Tournoux, 1988)  
24 and the Montreal Neurological Institute (MNI) atlas (Evans et al., 1992) have become fundamental  
25 pillars for performing group analysis and anatomical segmentations such as the Automated  
26 Anatomical Labeling atlas (Tzourio-Mazoyer et al., 2002) are commonly used to report results of

1 regional outcomes of brain imaging data. A high-resolution human brain atlas of 5-HT receptors will  
2 represent a valuable tool for neuroimaging studies investigating the 5-HT system and disorders related  
3 to its dysfunction.

4 The distribution of 5-HT receptors in the human post-mortem brain has in the past been  
5 extensively described by autoradiography. However, autoradiography measurements, although  
6 quantitative, provide far less spatial information than a whole-brain atlas. With the development of  
7 well-validated radioligands for imaging the 5-HT system in vivo, it is now possible to image specific  
8 5-HT receptor subtypes and the 5-HT transporter. Up to now, specific and validated PET radioligands  
9 for use in humans have been developed for the receptors 5-HT<sub>1A</sub>R, 5-HT<sub>1B</sub>R, 5-HT<sub>2A</sub>R, 5-HT<sub>4</sub>R and  
10 for 5-HTT (Paterson and Kornum, 2013). A radioligand for the 5-HT<sub>6</sub> receptor has been validated in  
11 humans (Parker et al., 2012) but was not included here because it also has high affinity to the 5-HT<sub>2A</sub>  
12 receptor (Parker et al., 2015).

13 We here present an MRI- and PET-based high-resolution atlas of the human brain 5-HT  
14 receptors 5-HT<sub>1A</sub>R, 5-HT<sub>1B</sub>R, 5-HT<sub>2A</sub>R, 5-HT<sub>4</sub>R and the 5-HTT, represented both in volume and on  
15 the cortical surface. The atlas was generated using a subset of the Center for Integrated Molecular  
16 and Brain Imaging's (Cimbi) extensive database (Knudsen et al., 2015), including 210 healthy  
17 volunteers aged between 18 and 45 years. Regional PET binding values were compared to  
18 corresponding post-mortem autoradiography data (Bonaventure et al., 2000; Varnäs et al., 2004)  
19 allowing us to validate our results and convert binding values into densities. Furthermore, regional  
20 densities were compared with mRNA levels from the Allen Human Brain Atlas (Hawrylycz et al.,  
21 2012; French and Paus, 2015) to confirm previous findings and gain novel insights into the  
22 localization of the receptor/transporter protein versus its expression.

## 23 **Materials & Methods**

### 24 **Participants**

25 All participants included in this study were healthy male and female controls from the Cimbi  
26 database (Knudsen et al., 2015); all data from this database is freely accessible. The data analysis was

1 restricted to include individuals aged between 18 and 45 years. Participants were recruited by  
2 advertisement for different research protocols approved by the Ethics Committee of Copenhagen and  
3 Frederiksberg, Denmark. A total of 232 PET scans and corresponding structural MRI scans were  
4 acquired for 210 individual participants; 189 subjects had only 1 scan, 20 subjects had 2 scans and a  
5 single had 3 scans. Demographics details are presented in Table 1.

## 6 **Positron Emission Tomography and Structural MRI**

7 PET data was acquired in list-mode on a Siemens HRRT scanner operating in 3D-acquisition  
8 mode, with an approximate in-plane resolution of 2 mm (1.4 mm in the center of the field of view  
9 and 2.4 mm in cortex) (Olesen et al., 2009). PET frames were reconstructed using a 3D-OSEM-PSF  
10 algorithm (Comtat et al., 2008; Sureau et al., 2008). Scan time and frame length were designed  
11 according to the radiotracer characteristics. Dynamic PET frames were realigned using AIR 5.2.5  
12 (Woods et al., 1992). See Table 2 for details on framing and realignment. T1 and T2-weighted  
13 structural MRI were acquired on four different Siemens scanners with standard parameters. All  
14 structural MRIs (T1 & T2) were unwarped offline using FreeSurfer's gradient\_nonlin\_unwarp v0.8  
15 or online on the scanner (Jovicich et al., 2006). For further details on structural MRI acquisition  
16 parameters, see Knudsen et al. (2015).

17 Further processing was performed with FreeSurfer 5.3 (Fischl 2012,  
18 <http://surfer.nmr.mgh.harvard.edu>) using a surface and a volume stream. The individual cortical  
19 surfaces were reconstructed using the structural MRI corrected for gradient non-linearities. The pial  
20 surfaces were further refined using T2-weighted structural images and manually corrected where  
21 necessary. PET-MR coregistration was estimated using boundary-based registration (Greve and  
22 Fischl, 2009) between the time-weighted sum of the PET time-activity curves (TAC) and the  
23 structural MRI. Additionally, the transformation from individual MR space to normal MNI152 space  
24 was estimated with Combined Volume-Surface registration (Postelnicu et al., 2009) (CVS).

25 Regional TACs for the cortical regions were extracted by resampling the TACs to the cortical  
26 surface (Greve and Fischl, 2009) and taking the average within each of the 34 regions defined by the

1 Desikan-Killiany cortical atlas (Desikan et al., 2006) automatically labeled by FreeSurfer. Similarly,  
2 regional TACs for 7 subcortical regions were obtained by resampling the TACs to an MR-based  
3 refined version of the automatic volume segmentation derived by FreeSurfer for each subjects as  
4 describe in Greve et al. (2016). Additionally, a segmentation of cerebellum including different lobules  
5 (e.g. vermis) were created using SUIT 2.7 (Diedrichsen, 2006) and SPM12  
6 (<http://www.fil.ion.ucl.ac.uk/spm>). Gray matter cerebellar segmentations used as reference region  
7 were created by limiting the FS segmentation to the intersection with the cerebellum labeled by SUIT,  
8 excluding vermis; this has the effect of removing peripheral overlabeling sometimes present in the  
9 cerebellar segmentations.

10 Due to the high binding of [<sup>11</sup>C]DASB and [<sup>11</sup>C]CUMI-101 within dorsal and median raphe,  
11 these ROIs can be delineated directly on PET images. Raphe TACs were obtained by delineating the  
12 ROIs on the time-weighted summed TACs using anatomical landmarks from structural MRI  
13 according to the method described in Beliveau et al. (Beliveau et al., 2015) and extracting the average  
14 TACs within these regions. For the other tracers, raphe TACs were obtained by taking the average  
15 within normalized dorsal and median raphe templates. These templates were created by transferring  
16 the raphe ROIs previously derived to common space (MNI152) using CVS and taking the voxels with  
17 the highest overlap with a target volume of 150 mm<sup>3</sup> and 100 mm<sup>3</sup> for dorsal and median raphe,  
18 respectively. The delineations and templates were transferred back to PET space using CVS.

19 Subcortical voxel-wise TACs in common volume space (MNI152) were obtained using CVS.  
20 Cortical vertex-wise TACs in common surface space (fsaverage) were obtained using the cortical-  
21 surface alignment estimated by FreeSurfer (Fischl et al., 1999). Finally, cortical and subcortical TACs  
22 were respectively surface smoothed by 10mm and volume smoothed by 5mm full width half  
23 maximum.

## 24 **Kinetic Modeling**

25 For all radioligands modeling of the parametric and regional BP<sub>ND</sub> was performed using the  
26 FS PET pipeline (Greve et al., 2013) with a Multilinear Reference Tissue Model 2 (MRTM2) (Ichise

1 et al., 2003) using cerebellar gray matter, excluding vermis, as a reference region .The reference  
2 region washout rate ( $k_2'$ ) was computed using MRTM (Ichise et al., 1996); the high-binding TAC  
3 was obtained from a surface-weighted average of neocortical regions for [ $^{11}\text{C}$ ]CUMI-101,  
4 [ $^{11}\text{C}$ ]AZ10419369 and [ $^{11}\text{C}$ ]Cimbi-36, and from a volume-weighted average of caudate and putamen  
5 for [ $^{11}\text{C}$ ]SB207145 and of caudate, putamen and thalamus for [ $^{11}\text{C}$ ]DASB. Parametric and regional  
6  $\text{BP}_{\text{ND}}$  were thresholded between 0 and 10 (outliers were set to the corresponding threshold value) and  
7 average maps were created. For 5-HTT, the TAC of the median raphe was found to be irreversible  
8 within the scan time, hence the  $\text{BP}_{\text{ND}}$  for this region is not reported and it was disregarded from further  
9 analysis.

## 10 **In Vivo Binding and Autoradiography**

11 In order to compare our results to those of Varnäs et al. (2004) and Bonaventure et al. (2000),  
12 regional values were adapted. First, the autoradiography data from Varnäs et al. was averaged across  
13 layers for individual cortical regions and divisions of subcortical structures were averaged to generate  
14 larger identifiable structures. Then each region of the Desikan-Killiany cortical atlas (both left and  
15 right independently) as well as each subcortical region were grouped according to a set of regions  
16 common to the autoradiography data. Regional  $\text{BP}_{\text{ND}}$  values were then averaged within group using  
17 a volume/surface-weighting. Regions where no reasonable pairing could be made were disregarded.  
18 The association between  $\text{BP}_{\text{ND}}$  and autoradiography was estimated using a linear regression without  
19 intercept, as a null density is expected to yield null binding, and the estimated slopes were used to  
20 transform  $\text{BP}_{\text{ND}}$  into density values. Pearson's and Spearman's correlation coefficients were also  
21 computed for all associations. The Shapiro-Wilks test was used to assess the normality of the residuals  
22 and the null-hypothesis of normality was rejected for  $p < 0.1$ ; whenever the residuals did not pass the  
23 test, only the Spearman's correlation coefficient is reported. Densities in units of pmol/g tissue were  
24 converted to pmol/ml using an approximate gray matter density of 1.045 g/ml (DiResta et al., 1991).

25 A linear mixed-effect model was used to investigate the global effect of age and gender on the  
26 regional density for the five 5-HT targets. The model included age, gender and the interaction between

1 age and gender as a fixed effect. Region-specific random effects were used to model regional-specific  
2 densities and subject-specific random effects to account for the correlation between the regional  
3 measurements of a given individual. To handle different variability in 5-HT density between regions,  
4 a separate variance parameter was estimated for each region. To investigate a possible regional-  
5 specific effect of age or gender, a separate linear regression was fitted to each region including age,  
6 gender and a possible interaction between age and gender as covariates. In the global models, the p-  
7 values were adjusted for multiple comparison over tracers (n=5) controlling the false discovery at 5%  
8 (Benjamini and Hochberg, 1995). Similarly, regional models were corrected for multiple comparison  
9 over regions (n=42). For the entire analysis, the significance threshold was fixed at  $p < 0.05$ . Regional  
10 densities were averaged for left and right hemispheres.

11 The  $BP_{ND}$  of small volume of interest surrounded by low binding tissue can be drastically  
12 underestimated due to partial volume effects. As previously described (Savli et al., 2012), this is  
13 particularly pronounced in the raphe nuclei for the 5-HTT and 5-HT<sub>1A</sub>R as there is high binding for  
14 the corresponding radioligand in this region, but much lower levels in to neighboring white matter  
15 tissue of the brainstem. Accordingly, the raphe nuclei density values reported here should be  
16 interpreted with caution and, although they are depicted in Figure 1 and 5, this region was excluded  
17 from any quantitative analysis for the 5-HTT and the 5-HT<sub>1A</sub>R. Similarly, the 5-HTT  $BP_{ND}$   
18 distribution within globus pallidus was found to be highly heterogeneous due to partial volume effect  
19 from the caudate, hence this region was also excluded from quantitative analysis for the 5-HTT.

## 20 **In Vivo Binding and mRNA Levels**

21 Regional binding values were compared to 5-HT receptors and transporter mRNA normalized  
22 expression values from the Allen Human Brain Atlas (Hawrylycz et al., 2012). The atlas contains  
23 probe information from 6 human brains. Each probe is associated with mRNA levels (log<sub>2</sub> intensity)  
24 for all genes sequenced, an anatomical label and coordinates in the MNI152 space, as well as many  
25 other parameters. For more details on the material and methods for the Allen Human Brain Atlas, see  
26 the Microarray Survey Technical White papers available at (<http://help.brain->

1 [map.org/display/humanbrain/Documentation](http://map.org/display/humanbrain/Documentation)). mRNA expression values for regions of the Desikan-  
2 Killiany cortical atlas were obtained from the work of French and Paus (2015). Each probe of the  
3 Allen Human Brain Atlas was paired to a cortical region using its coordinates in the MNI152 space  
4 and regional expression values were obtained by averaging expression values across probes, and then  
5 by taking the median per regions and finally taking the median across subjects. We used the same  
6 approach to obtain subcortical expression values, however probes were paired to subcortical regions  
7 directly by their anatomical label rather than using their coordinates to identify corresponding regions.  
8 Both binding values and mRNA values were averaged between left and right hemispheres. As above,  
9 the association between binding and mRNA was estimated using a linear regression and Pearson's  
10 and Spearman's correlation coefficients were also computed for all association. Dorsal raphe was  
11 excluded from the regression for 5-HTT and 5-HT<sub>1A</sub>R and the regression was performed for cortical  
12 regions only for the 5-HT<sub>2A</sub>R. For 5-HT<sub>1B</sub>R and 5-HT<sub>2A</sub>R subcortical regions exhibited patterns  
13 distinct from the cortical regions, hence the analysis was stratified between cortical and subcortical  
14 regions for these two targets.

## 15 **Results**

### 16 **In Vivo Molecular Imaging and Autoradiography**

17 Brain regional BP<sub>ND</sub> values were compared to the corresponding receptor density  
18 measurements from post-mortem autoradiography data from Varnäs et al. (2004) and Bonaventure et  
19 al. (2000) (for 5-HT<sub>4</sub>R). Figure 1 (A-E) shows the relation between autoradiography  
20 receptor/transporter B<sub>max</sub> from the two studies and PET measures of BP<sub>ND</sub> from the Cimbi database.  
21 For all five targets, we found good to excellent associations between BP<sub>ND</sub> and B<sub>max</sub>, with Pearson's  
22 correlation coefficients ranging from 0.88 to 0.97 and Spearman's correlation coefficients ranging  
23 from 0.72 to 0.97. For 5-HTT, the residuals for 5-HTT did not pass the Shapiro-Wilks test for  
24 normality, hence the Pearson's correlation is not reported for that association. The slope estimates of  
25 the regression were used to transform the BP<sub>ND</sub> atlases into B<sub>max</sub> atlases (Figure 2 and 3), allowing

1 for a direct comparison across targets. The regional densities are presented in Figure 4. No global or  
2 regional significant effect of age, gender or their interaction was found.

### 3 **Receptor Density and mRNA**

4 The associations between in vivo receptor density, obtained by converting  $BP_{ND}$  into densities,  
5 and mRNA levels are shown in Figure 5. For the 5-HT<sub>1A</sub>R, we found excellent correlation between  
6 the protein densities and mRNA levels, with Pearson's and Spearman's correlation coefficients of  
7 0.94 and of 0.94, respectively. For 5-HT<sub>4</sub>, the residuals did not pass the Shapiro-Wilks test for  
8 normality, but we found a moderate Spearman's correlation coefficient of 0.50. The 5-HT<sub>1B</sub>R and 5-  
9 HT<sub>2A</sub>R showed a distinctly different pattern compared to other targets, with good Pearson's  
10 correlation coefficients (0.66 and 0.60, respectively) and weak to moderate Spearman's correlation  
11 coefficients (0.28 and 0.46) in cortical regions, but there was no statistically significant correlation in  
12 subcortical regions.

## **DISCUSSION**

13 We here present the first high-resolution PET- and MR-based in vivo human brain atlas of  
14 four 5-HT receptors and the transporter. The atlas highlights key features of the 5-HT targets; their  
15 spatial distribution and abundance relative to each other. As we identified high correlations with post-  
16 mortem autoradiography receptor measurements, the atlas could be calibrated to represent absolute  
17 receptor or transporter densities, thus making the atlas independent of the PET methodology in terms  
18 of choice of radiotracer and modeling approach. Access to such a high-resolution atlas of the 5-HT  
19 system enables scientists not only to evaluate the absolute densities of the individual targets, but also  
20 the relative abundance of protein, and in any brain region of interest. A few caveats with this approach  
21 deserve, however, to be mentioned here. Whereas autoradiography provides a measurement of the  
22 target density, PET returns an outcome measure that is proportional to the density of the target  
23 available for radioligand binding, and the measure most notably depends on the in vivo radioligand  
24 affinity to the target. However, since the occupancy of endogenous 5-HT is low for most targets

1 (Paterson et al., 2010) it is unlikely that individual differences in endogenous 5-HT (and thereby in  
2 vivo affinity) would incur any bias.

3         Although PET imaging offers unique sensitivity and specificity, the intrinsic image resolution  
4 of PET is lower than for MRI. A prior brain 5-HT atlas has been reported based on PET scanners with  
5 a resolution of 4.4 mm and was generated independent of anatomical MRI (Savli et al., 2012).  
6 Leveraging high-resolution structural MRI (~1 mm resolution) in combination with molecular images  
7 acquired with a high-resolution PET scanner with a resolution of 2 mm allows for precise  
8 segmentation of brain regions and accurate inter-subject normalization. The surface-based approach  
9 used in this work has also been shown to lead to a reduction in bias and variance of PET-derived  
10 measurements (Greve et al., 2013). A main advantage of the surface-based method is to diminish  
11 partial volume effects introduced by smoothing in the volume; smoothing on the surface drastically  
12 reduces the blurring of neighboring tissues with cortical gray matter as well as blurring across  
13 adjacent gyri (Jr et al., 2006). Nevertheless, we still see subtle signs suggestive of partial volume  
14 effects, e.g., bands of lower binding along the medial wall, see Figure 6. Although a partial volume  
15 corrected atlas could be generated, we chose not to do so because methods for partial volume  
16 corrections come with their own set of limitations (Harri et al., 2007) and can lead to different results  
17 depending on the algorithm used (Greve et al., 2016).

18         Although [<sup>11</sup>C]Cimbi-36 has been shown to have some affinity for 5-HT<sub>2C</sub>, these receptors are  
19 mostly limited to the choroid plexus and the hippocampus. Furthermore, binding measures for  
20 [<sup>11</sup>C]Cimbi-36 have been shown to be very strongly correlated to those of the 5-HT<sub>2A</sub> antagonist  
21 radiotracer [<sup>18</sup>F]Altanserin (Ettrup et al., 2016). Hence, any bias caused by the contribution of 5-HT<sub>2C</sub>  
22 receptors is expected to have minimal impact on the results presented here.

23         We compared our in vivo imaging atlases to meticulous autoradiography studies of the  
24 relevant 5-HT targets in postmortem human brain slices (Bonaventure et al., 2000; Varnäs et al., 2004).  
25 The postmortem brains in Varnäs et al. (2004) and Bonaventure et al. (2000) were retrieved from  
26 individuals older than those included in our study, with respective mean age of 58 and 55 versus 26

1 years in our cohort. Thus, the atlas densities represent those that can be observed in individuals  
2 matching the mean age of the population in the autoradiography studies. Within the current cohort,  
3 we did not observe any significant effect of age or gender within our data, most likely because of the  
4 limited age range of the subjects. Whereas some 5-HT targets, such as 5-HT<sub>1B</sub>R and 5-HT<sub>2A</sub>R, are  
5 relatively independent of age others, have been shown to have a pronounced age-dependent decline  
6 and/or sex-differences (Moses-kolko et al., 2011; Nord et al., 2014). Hence, minor data adjustments  
7 may be necessary when relating these atlases to specific research questions.

8 For all the serotonergic targets, except for the 5-HT<sub>1A</sub>R (Rizzo et al., 2014), we provide novel  
9 information about the relationship between in vivo molecular imaging in humans and the associated  
10 mRNA levels assessed in postmortem human brain tissue. The relation between the cerebral 5-HT  
11 target densities and their corresponding mRNA levels is of interest as mRNA levels often do not  
12 correspond to their protein levels because protein concentrations depend on the relative rates of  
13 transcription, mRNA decay, translation, and protein degradation (Vogel et al., 2010). Relating the two  
14 measures in brain space generates important information about the gene-protein translation. A high  
15 spatial correspondence between the two measures suggests that the protein is located on or at least  
16 close to the cell body where the protein synthesis takes place. We found no significant association  
17 between 5-HTT mRNA and 5-HTT density although as expected, both were high in the dorsal raphe  
18 (Figure 5, A). This is consistent with the exclusively presynaptic localization of 5-HTT and hence  
19 primary mRNA localization within raphe nuclei (Hoffman et al., 1998) and 5-HTT protein being  
20 located on terminal projections distant from 5-HT neurons (Zhou et al., 1998). The 5-HTT mRNA  
21 levels were overall low, both relative to the mRNA of other targets and to the 5-HTT protein density.  
22 Consistent with Rizzo et al. (2014), we find a very strong association between 5-HT<sub>1A</sub>R mRNA and  
23 5-HT<sub>1A</sub>R protein density as determined with in vivo molecular neuroimaging (Figure 5, B). Rizzo  
24 and colleagues ascribed the tight correlation to a more general feature of the serotonergic system but  
25 here we show that several other serotonergic targets show profound regional differences. We found a  
26 fair association between neocortical 5-HT<sub>1B</sub>R mRNA and 5-HT<sub>1B</sub>R density (Figure 5, C) but the

1 subcortical regions did not conform to this association. As for the latter, our findings are consistent  
2 with a previous postmortem human brain study where proportionally higher levels of 5-HT<sub>1B</sub>R  
3 mRNA than protein were found particularly in the ventral striatum, whereas the pallidum which is  
4 the brain region with the highest 5-HT<sub>1B</sub>R density had low mRNA levels (Varnäs et al., 2005). This  
5 supports the observation in rodents that 5-HT<sub>1B</sub>R in pallidum are localized in nerve terminals from  
6 striatal projections (Boschert et al., 1994), that are of GABAergic origin (Ghavami et al., 1999). To  
7 the best of our knowledge, existing literature does not provide evidence about the relative densities  
8 of 5-HT<sub>1B</sub>R autoreceptors and heteroreceptors in different brain regions but due to the specific pattern  
9 observed here, we speculate that the 5-HT<sub>1B</sub>R heteroreceptors may be relatively more abundant in  
10 subcortical regions. An interesting pattern of 5-HT<sub>2A</sub>R mRNA versus 5-HT<sub>2A</sub>R density emerged:  
11 whereas the neocortical brain regions showed a good, linear correlation, there was no association  
12 between the two measures in subcortical brain regions (Figure 5, D) and the neocortical and  
13 subcortical regions fall in two separate clusters on the graph. The pattern is in agreement with  
14 observations in the macaque monkey brain (López-Giménez et al., 2001) and suggests that the  
15 regulation and role of the 5-HT<sub>2A</sub>R markedly differs between neocortical and subcortical brain  
16 regions, possibly because the 5-HT<sub>2A</sub>R in neocortex are located in the apical part of pyramidal  
17 neurons (Jakab and Goldman-Rakic, 2000). In addition, the 5-HT<sub>2A</sub>R mRNA levels are almost twice  
18 as high compared to the other investigated targets. We speculate that high mRNA levels enable the  
19 system to quickly regulate synaptic 5-HT<sub>2A</sub>R levels, consistent with the ligand-induced endocytosis  
20 and recycling of 5-HT<sub>2A</sub>R (Raote et al., 2013). We observed a moderate correlation association  
21 between 5-HT<sub>4</sub>R mRNA and 5-HT<sub>4</sub>R protein density (Figure 5, E). This finding is consistent with  
22 data obtained in human, where 5-HT<sub>4</sub>R mRNA levels and densities were high in caudate, putamen,  
23 accumbens and the hippocampus formation, and were both relatively lower in other brain regions.

## 24 **Conclusion**

25 We here present a comprehensive PET- and MR-based high-resolution brain atlas of the  
26 serotonin system. By combining the *in vivo* atlases with postmortem autoradiography measurements,

1 we calibrated the individual atlas to represent quantitative protein levels in terms of pmol/ml.  
2 Furthermore, we describe the relation between regional serotonergic target densities and their mRNA  
3 levels, some for the first time in humans. The approach is generally applicable for any molecular  
4 target that can be visualized in vivo by PET. Such publicly available in vivo human brain atlases will  
5 serve as an important resource for neuroscience.  
6

## 1 REFERENCES

- 2 Beliveau V, Svarer C, Frokjaer VG, Knudsen GM, Greve DN, Fisher PM (2015) Functional  
3 connectivity of the dorsal and median raphe nuclei at rest. *Neuroimage* 116:187–195.
- 4 Benjamini Y, Hochberg Y (1995) Controlling the false discovery rate: a practical and powerful  
5 approach to multiple testing. *J R Stat Soc Ser B* 57:289–300.
- 6 Bonaventure P, Hall H, Gommeren W, Cras P, Langlois X, Jurzak M, Leysen JE (2000) Mapping of  
7 serotonin 5-HT<sub>4</sub> receptor mRNA and ligand binding sites in the post-mortem human brain.  
8 *Synapse* 36:35–46.
- 9 Boschert U, Amara DA, Segu L, Hen R (1994) The mouse 5-hydroxytryptamine<sub>1B</sub> receptor is  
10 localized predominantly on axon terminals. *Neuroscience* 58:167–182.
- 11 Comtat C, Sureau FC, Sibomana M, Hong IK, Sjöholm N, Trebossen R (2008) Image based  
12 resolution modeling for the HRRT OSEM reconstructions software. In: 2008 IEEE Nuclear  
13 Science Symposium Conference Record, pp 4120–4123. IEEE.
- 14 Cryan JF, Harkin A, Naughton M, Kelly JP, Leonard BE (2000) Characterization of D -  
15 fenfluramine-induced hypothermia: evidence for multiple sites of action. *Eur J Pharmacol*  
16 390:275–285.
- 17 Desikan RS, Ségonne F, Fischl B, Quinn BT, Dickerson BC, Blacker D, Buckner RL, Dale AM,  
18 Maguire RP, Hyman BT, Albert MS, Killiany RJ (2006) An automated labeling system for  
19 subdividing the human cerebral cortex on MRI scans into gyral based regions of interest.  
20 *Neuroimage* 31:968–980.
- 21 Diedrichsen JJ (2006) A spatially unbiased atlas template of the human cerebellum. *Neuroimage*  
22 33:127–138.
- 23 DiResta GR, Lee J, Arbit E (1991) Measurement of brain tissue specific gravity using pycnometry.  
24 *J Neurosci Methods* 39:245–251.
- 25 Dorocic IP, Fürth D, Xuan Y, Johansson Y, Pozzi L, Silberberg G, Carlén M, Meletis K (2014) A  
26 Whole-Brain Atlas of Inputs to Serotonergic Neurons of the Dorsal and Median Raphe Nuclei.  
27 *Neuron* 83:663–678.
- 28 Ettrup A, Svarer C, McMahon B, da Cunha-Bang S, Lehel S, Møller K, Dyssegaard A, Ganz M,  
29 Beliveau V, Jørgensen LM, Gillings N, Knudsen GM (2016) Serotonin 2A receptor agonist  
30 binding in the human brain with [(11)C]Cimbi-36: Test-retest reproducibility and head-to-head  
31 comparison with the antagonist [(18)F]altanserin. *Neuroimage* 34:1188–1196.
- 32 Evans AC, Collins DL, Milner B (1992) An MRI- Based Stereotactic Atlas from 250 Young Normal  
33 Subjects. *Soc Neurosci Abstr* 18:408.
- 34 Fischl B (2012) FreeSurfer. *Neuroimage* 62:774–781.
- 35 Fischl B, Sereno MI, Tootell RBH, Dale AM (1999) High-resolution intersubject averaging and a  
36 coordinate system for the cortical surface. *Hum Brain Mapp* 8:272–284.
- 37 French L, Paus T (2015) A FreeSurfer view of the cortical transcriptome generated from the Allen  
38 Human Brain Atlas. *Front Neurosci* 9:1–5.
- 39 Ghavami a, Stark KL, Jareb M, Ramboz S, Ségu L, Hen R (1999) Differential addressing of 5-  
40 HT<sub>1A</sub> and 5-HT<sub>1B</sub> receptors in epithelial cells and neurons. *J Cell Sci* 112 Pt 6:967–976.
- 41 Greve DN, Fischl B (2009) Accurate and robust brain image alignment using boundary-based  
42 registration. *Neuroimage* 48:63–72.
- 43 Greve DN, Salat DH, Bowen SL, Izquierdo-Garcia D, Schultz AP, Catana C, Becker JA, Svarer C,  
44 Knudsen G, Sperling RA, Johnson KA (2016) Different partial volume correction methods  
45 lead to different conclusions: An 18F-FDG PET Study of aging. *Neuroimage* 132:334–343.
- 46 Greve DN, Svarer C, Fisher PM, Feng L, Hansen AE, Baare W, Rosen B, Fischl B, Knudsen GM  
47 (2013) Cortical surface-based analysis reduces bias and variance in kinetic modeling of brain  
48 PET data. *Neuroimage* 92C:225–236.
- 49 Hannon J, Hoyer D (2008) Molecular biology of 5-HT receptors. *Behav Brain Res* 195:198–213.
- 50 Harri M, Mika T, Jussi H, Nevalainen OS, Jarmo H (2007) Evaluation of partial volume effect  
51 correction methods for brain positron emission tomography: Quantification and

1 reproducibility. *J Med Phys* 32:108–117.

2 Hawrylycz MJ et al. (2012) An anatomically comprehensive atlas of the adult human brain  
3 transcriptome. *Nature* 489:391–399.

4 Hoffman BJ, Hansson SR, Mezey E, Palkovits M (1998) Localization and dynamic regulation of  
5 biogenic amine transporters in the mammalian central nervous system. *Front Neuroendocrinol*  
6 19:187–231.

7 Ichise M, Ballinger J, Golan H (1996) Noninvasive quantification of dopamine D2 receptors with  
8 iodine-123-IBF SPECT. *J Nucl Med* 37:513–520.

9 Ichise M, Liow J, Lu J, Takano A (2003) Reference Tissue Parametric Imaging Methods:  
10 Application to [<sup>11</sup>C] DASB Positron Emission Tomography Studies of the Serotonin  
11 Transporter in. *J Cereb blood flow Metab* 23:1096–1112.

12 Jakab RL, Goldman-Rakic PS (2000) Segregation of serotonin 5-HT<sub>2A</sub> and 5-HT<sub>3</sub> receptors in  
13 inhibitory circuits of the primate cerebral cortex. *J Comp Neurol* 417:337–348.

14 Jovicich J, Czanner S, Greve D, Haley E, van der Kouwe A, Gollub R, Kennedy D, Schmitt F,  
15 Brown G, Macfall J, Fischl B, Dale A (2006) Reliability in multi-site structural MRI studies:  
16 effects of gradient non-linearity correction on phantom and human data. *Neuroimage* 30:436–  
17 443.

18 Jr DH, Saygin A, Sereno M, Hagler D (2006) Smoothing and cluster thresholding for cortical  
19 surface-based group analysis of fMRI data. *Neuroimage* 33:1093–1103.

20 Knudsen GM et al. (2015) The Center for Integrated Molecular Brain Imaging (Cimbi) Database.  
21 *Neuroimage*:1–7.

22 López-Giménez J, Vilaro TM, Palacios JM, Mengod G (2001) Mapping of 5-HT<sub>2A</sub> receptors and  
23 their mRNA in monkey brain: [<sup>3</sup>H]MDL100,907 autoradiography and in situ hybridization  
24 studies. *J Comp Neurol* 429:571–589.

25 Magalhães CP, de Freitas MFL, Nogueira MI, Campina RCDF, Takase LF, de Souza SL, de Castro  
26 RM (2010) Modulatory role of serotonin on feeding behavior. *Nutr Neurosci* 13:246–255.

27 Meneses A (1999) 5-HT system and cognition. *Neurosci Biobehav Rev* 23:1111–1125.

28 Moses-kolko EL, Price JC, Shah N, Berga S, Sereika SM, Fisher PM, Coleman R, Becker C, Mason  
29 NS, Loucks T, Meltzer CC (2011) Age , Sex , and Reproductive Hormone Effects on Brain  
30 Serotonin-1A and Serotonin-2A Receptor Binding in a Healthy Population.  
31 *Neuropsychopharmacology* 36:2729–2740.

32 Nord M, Cselenyi Z, Forsberg A, Rosenqvist G, Tiger M, Lundberg J, Varrone A, Farde L (2014)  
33 Distinct regional age effects on [<sup>11</sup>C]AZ10419369 binding to 5-HT<sub>1B</sub> receptors in the human  
34 brain. *Neuroimage* 103:303–308.

35 Oades RD (2010) *Handbook of the Behavioral Neurobiology of Serotonin*.

36 Olesen OV, Sibomana M, Keller SH, Andersen F, Jensen J, Holm S, Svarer C, Højgaard L (2009)  
37 Spatial resolution of the HRRT PET scanner using 3D-OSEM PSF reconstruction. *IEEE Nucl*  
38 *Sci Symp Conf Rec*:3789–3790.

39 Parker C a., Gunn RN, Rabiner E a., Slifstein M, Comley R, Salinas C, Johnson CN, Jakobsen S,  
40 Houle S, Laruelle M, Cunningham VJ, Martarello L (2012) Radiosynthesis and  
41 Characterization of <sup>11</sup>C-GSK215083 as a PET Radioligand for the 5-HT<sub>6</sub> Receptor. *J Nucl*  
42 *Med* 53:295–303.

43 Parker CA, Rabiner EA, Gunn R, Searle G, Martarello L, Comley R, Davy M, Wilson AA, Houle S,  
44 Mizrahi R, Laruelle M, Cunningham VJ (2015) Human kinetic modelling of the 5-HT<sub>6</sub> PET  
45 radioligand, <sup>11</sup>C-GSK215083, and its utility for determining occupancy at both 5HT<sub>6</sub> and  
46 5HT<sub>2A</sub> receptors by SB742457 as a potential therapeutic mechanism of action in Alzheimer’s  
47 disease. *J Nucl Med* 56:1901–1909.

48 Paterson L, Kornum B (2013) 5-HT radioligands for human brain imaging with PET and SPECT.  
49 *Med Res Rev* 33:54–111.

50 Paterson LM, Tyacke RJ, Nutt DJ, Knudsen GM (2010) Measuring endogenous 5-HT release by  
51 emission tomography: promises and pitfalls. *J Cereb Blood Flow Metab* 30:1682–1706.

52 Portas CM, Bjorvatn B, Ursin R (2000) Serotonin and the sleep/wake cycle : special emphasis on

1 microdialysis studies. *Prog Neurobiol* 60:12–35.

2 Postelnicu G, Zollei L, Fischl B (2009) Combined volumetric and surface registration. *Med*  
3 *Imaging, IEEE Trans* 28:508–522.

4 Raote I, Bhattacharyya S, Panicker MM (2013) Functional Selectivity in Serotonin Receptor 2A (5-  
5 HT2A) Endocytosis, Recycling, and Phosphorylation. *Mol Pharmacol* 83:42–50.

6 Rizzo G, Veronese M, Heckemann RA, Selvaraj S, Howes OD, Hammers A, Turkheimer FE,  
7 Bertoldo A (2014) The predictive power of brain mRNA mappings for in vivo protein density:  
8 a positron emission tomography correlation study. *J Cereb Blood Flow Metab* 34:827–835.

9 Savli M, Bauer A, Mitterhauser M, Ding Y (2012) Normative database of the serotonergic system in  
10 healthy subjects using multi-tracer PET. *Neuroimage* 63:447–459.

11 Sureau FC, Reader AJ, Comtat C, Leroy C, Ribeiro M-J, Buvat I, Trébossen R (2008) Impact of  
12 image-space resolution modeling for studies with the high-resolution research tomograph. *J*  
13 *Nucl Med* 49:1000–1008.

14 Talairach J, Tournoux P (1988) Co-planar stereotaxic atlas of the human brain: 3-dimensional  
15 proportional system: an approach to cerebral imaging.

16 Tzourio-Mazoyer N, Landeau B, Papathanassiou D, Crivello F, Etard O, Delcroix N, Mazoyer B,  
17 Joliot M (2002) Automated anatomical labeling of activations in SPM using a macroscopic  
18 anatomical parcellation of the MNI MRI single-subject brain. *Neuroimage* 15:273–289.

19 Varnäs K, Halldin C, Hall H (2004) Autoradiographic distribution of serotonin transporters and  
20 receptor subtypes in human brain. *Hum Brain Mapp* 22:246–260.

21 Varnäs K, Hurd YL, Hall H (2005) Regional expression of 5-HT1B receptor mRNA in the human  
22 brain. *Synapse* 56:21–28.

23 Vogel C, Abreu R de S, Ko D, Le S-YY, Shapiro BA, Burns SC, Sandhu D, Boutz DR, Marcotte  
24 EM, Penalva LO (2010) Sequence signatures and mRNA concentration can explain two-thirds  
25 of protein abundance variation in a human cell line. *TL - 6. Mol Syst Biol* 6:400.

26 Waldinger MD (2015) *Psychiatric disorders and sexual dysfunction.*, 1st ed. Elsevier B.V.

27 Woods RP, Cherry SR, Mazziotta JC (1992) Rapid automated algorithm for aligning and reslicing  
28 PET images. *J Comput Assist Tomogr* 16:620–633.

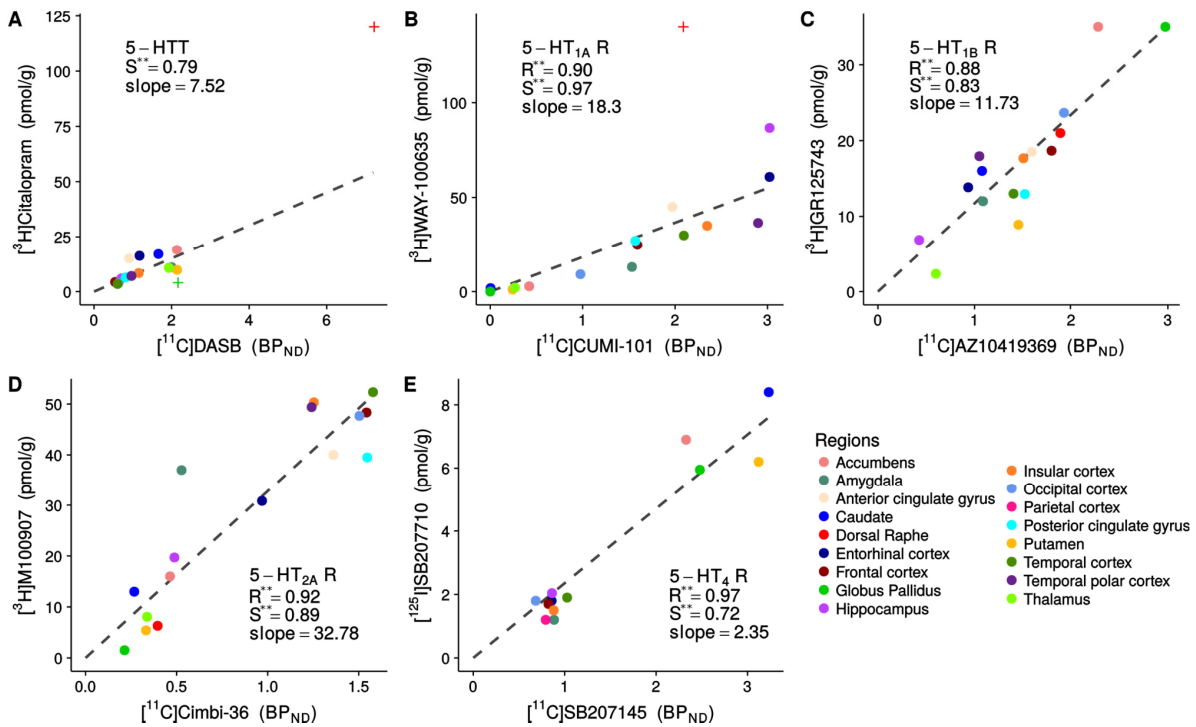
29 Young S, Leyton M (2002) The role of serotonin in human mood and social interaction: insight  
30 from altered tryptophan levels. *Pharmacol Biochem Behav* 71:857–865.

31 Zhou FC, Tao-Cheng JH, Segu L, Patel T, Wang Y (1998) Serotonin transporters are located on the  
32 axons beyond the synaptic junctions: anatomical and functional evidence. *Brain Res* 805:241–  
33 254.

34

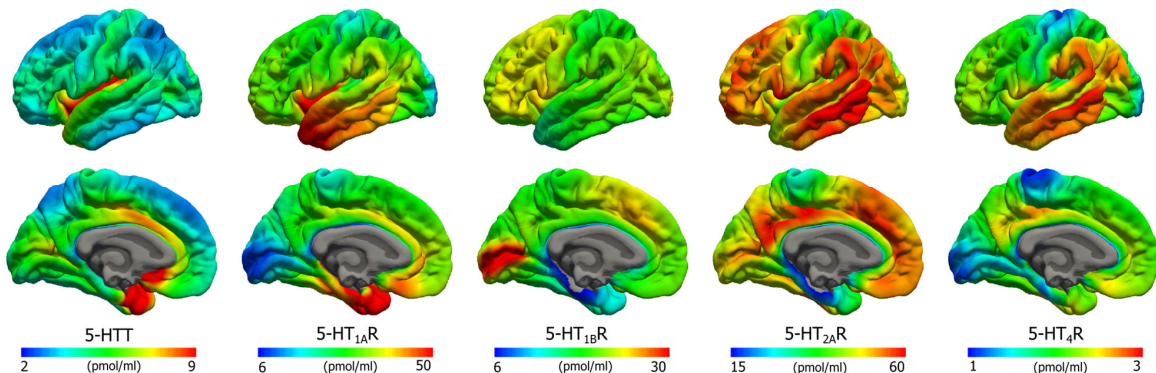
35

# 1 FIGURES AND TABLE LEGENDS



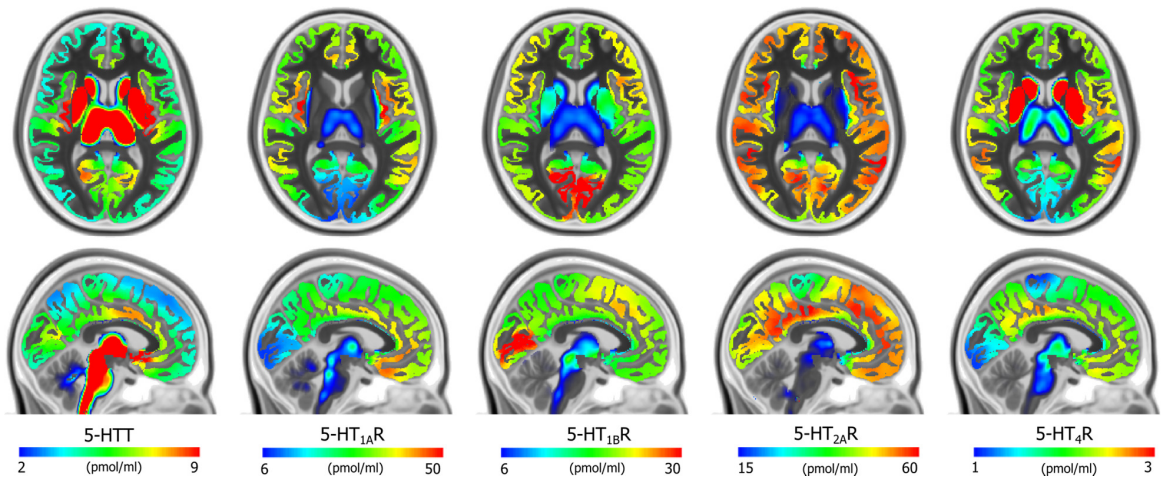
2

3 **Figure 1.** Regional BP<sub>ND</sub> and B<sub>max</sub> values for the five 5-HT targets. The regions in the PET image  
 4 space were combined to match the regions used by Varnäs et al. (2004) and Bonaventure et al.  
 5 (2000) in their autoradiography measurement. The regressions (fixed through 0.0) are shown as  
 6 black, dashed lines and the Pearson's (R) and Spearman's (S) correlation coefficients are reported;  
 7 \*\* indicate p<0.001. Dorsal raphe, median raphe and globus pallidus for 5-HTT and dorsal raphe  
 8 for 5-HT<sub>1A</sub>R were excluded from the regressions and marked with + on the figure, see the Material  
 9 & Methods section.

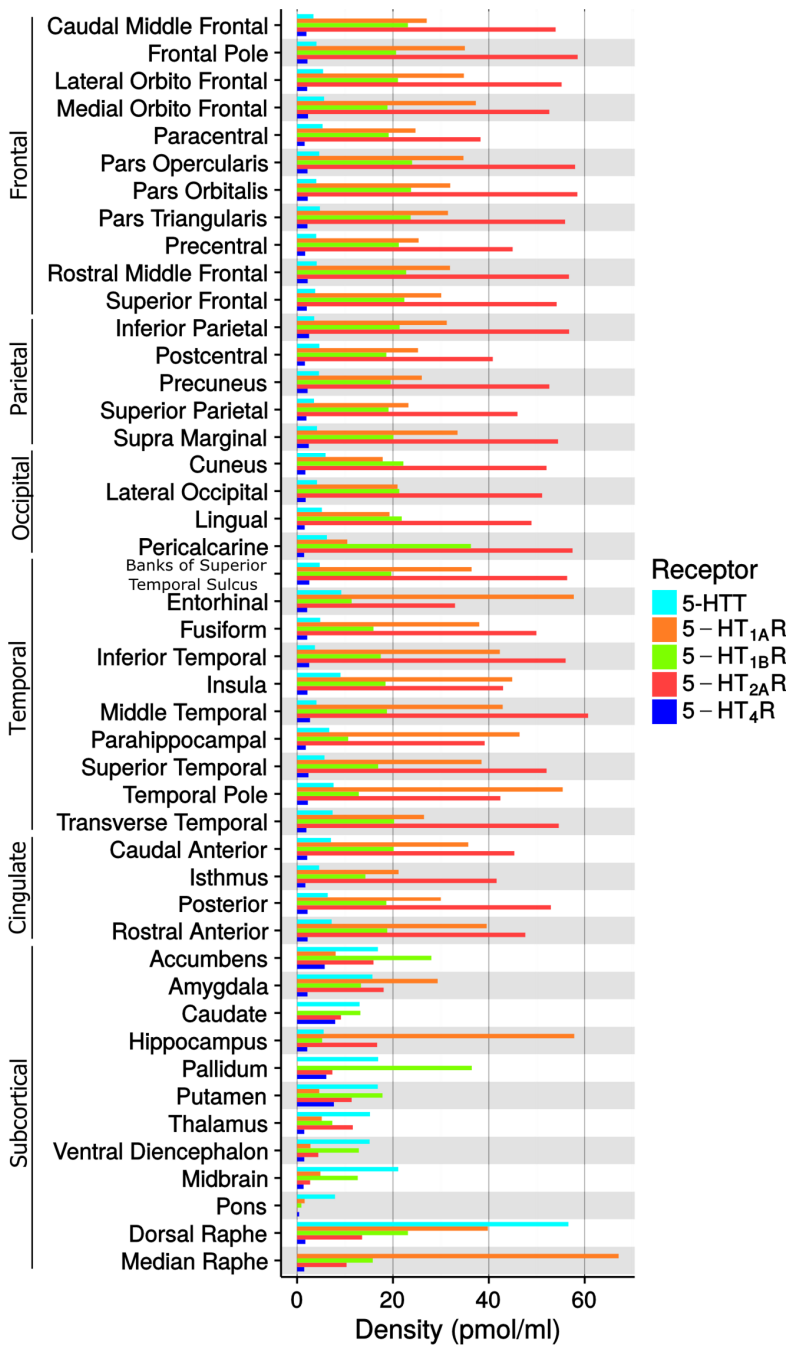


10

11 **Figure 2.** Average density (B<sub>max</sub>) maps for five 5-HT targets on the common FreeSurfer surface (left  
 12 hemisphere; lateral view, upper and medial view, lower). Color scaling was individually adjusted in  
 13 order to highlight features of the distributions.



2 **Figure 3.** Average density ( $B_{\max}$ ) maps for the five 5-HT targets in the common MNI152 space  
 3 (coronal, upper,  $z=8\text{mm}$  and sagittal, lower,  $x=-3\text{mm}$ ). Color scaling was individually adjusted to  
 4 highlight features of the distributions.

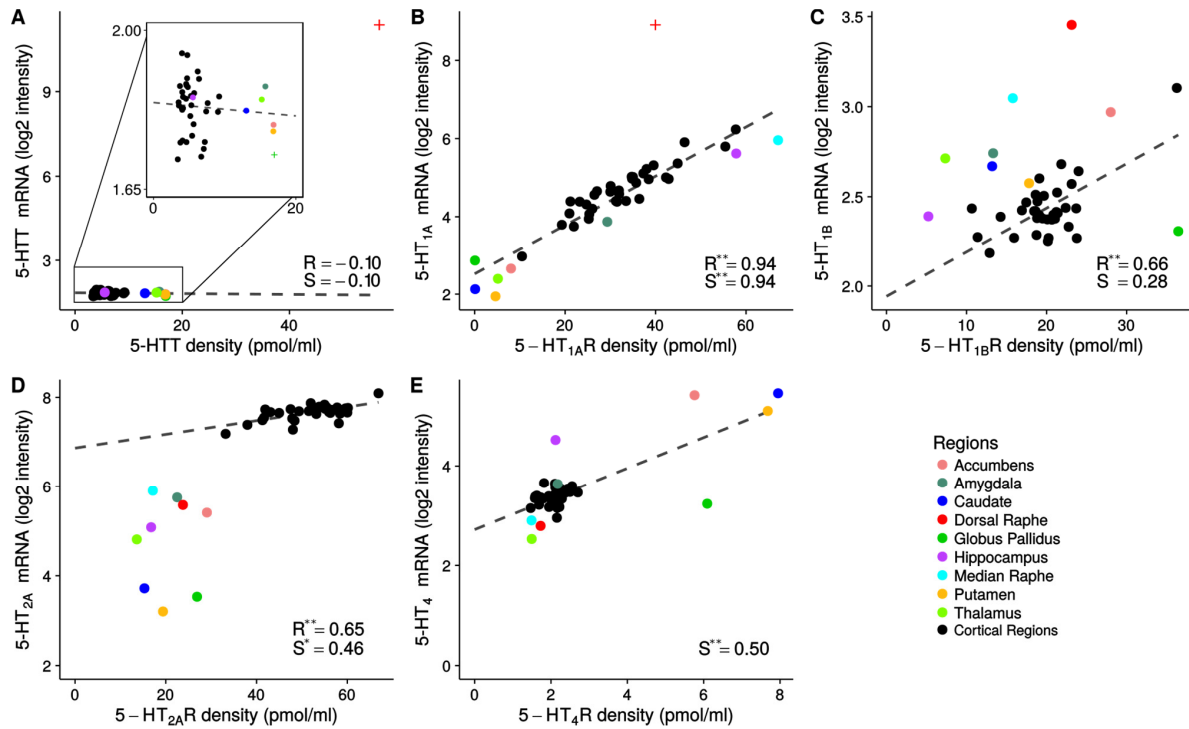


1

2 **Figure 4.** Density values ( $B_{max}$ ) of the five 5-HT targets in FreeSurfer defined brain regions.

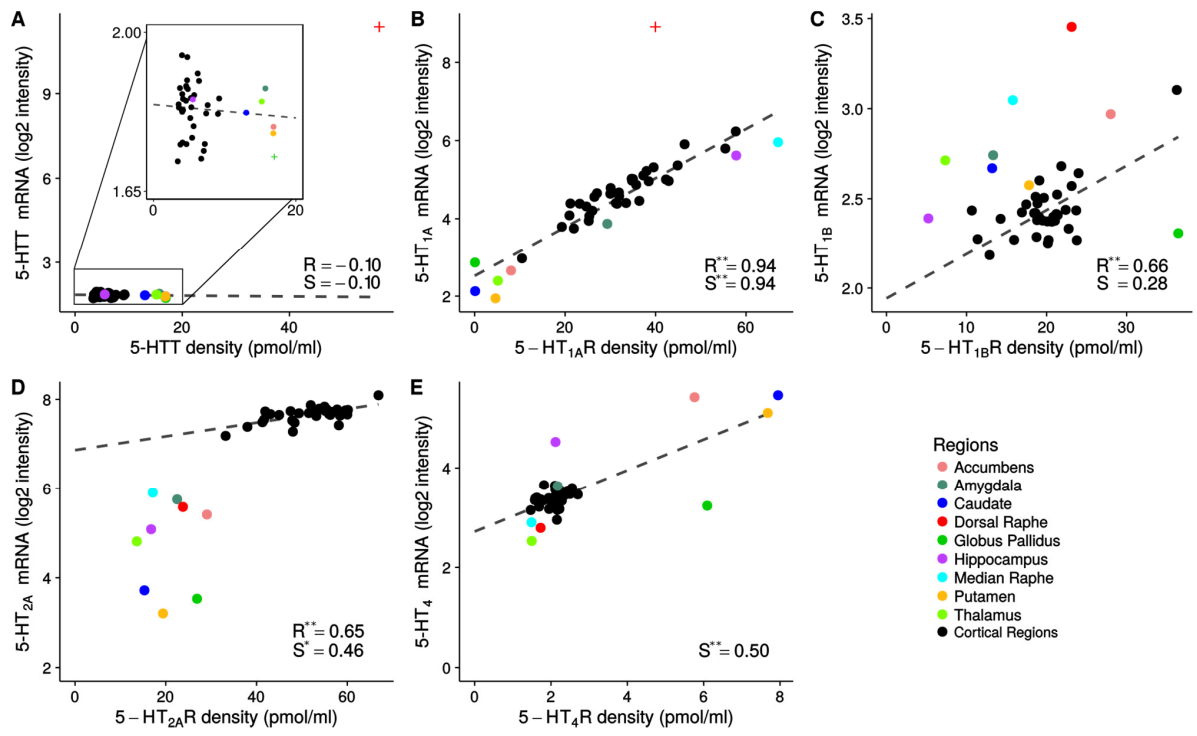
3 Median raphe is not reported for 5-HTT due the irreversible kinetic of the TACs, see also the

4 Material & Methods section.



1

2 **Figure 5.** Regional density values ( $B_{max}$ ) and mRNA levels for the five 5-HT targets. Subcortical  
3 data is shown in color and cortical data is shown in black. The regression lines are shown as black  
4 dashed lines and the Pearson's (R) and Spearman's (S) correlation coefficients are reported; \* and  
5 \*\* indicate  $p < 0.01$  and  $p < 0.001$ , respectively. In panel C and D, a line was fitted to cortical regions  
6 (black) only. Dorsal raphe, median raphe and globus pallidus for 5-HTT and dorsal raphe for 5-  
7 HT<sub>1A</sub>R were excluded from the regressions and marked with + on the figure, see also the Material  
8 & Methods section.



1

2 **Figure 6.** Average density ( $B_{max}$ ) maps for five 5-HT targets on the inflated common FreeSurfer  
 3 surface (left hemisphere; lateral view, upper and medial view, lower).

4

1 **TABLES**

2

3 **Table 1.** Demographics of the healthy individuals.

Receptor/transporter	5-HTT	5-HT <sub>1A</sub> R	5-HT <sub>1B</sub> R	5-HT <sub>2A</sub> R	5-HT <sub>4</sub> R
Radioligand	[ <sup>11</sup> C]DASB	[ <sup>11</sup> C]CUMI-101	[ <sup>11</sup> C]AZ10419369	[ <sup>11</sup> C]Cimbi-36	[ <sup>11</sup> C]SB207145
N	100	8	36	29	59
Gender (M/F)	29/71	3/5	24/12	15/14	41/18
Age (mean±sd)	25.1±5.8	28.4±8.8	27.8±6.9	22.6±2.7	25.9±5.3
BMI (kg/m <sup>2</sup> ) (mean±sd)	23.2±2.9	22.7±2.6	24.9±4.3	23.4±2.4	23.5±3.3
Injected dose (MBq) (mean±sd)	586.0±32.2	510.5±149.1	585.4±37.4	510.4±109.7	577.1±70.9
Injected Mass (µg) (mean±sd)	1.9±2.2	2.0±1.5	1.2±1.0	0.8±0.5	1.1±0.7

4

5

6 **Table 2.** PET scanning and realignment parameters.

7

Radioligand	[ <sup>11</sup> C]DASB	[ <sup>11</sup> C]CUMI-101	[ <sup>11</sup> C]AZ10419369	[ <sup>11</sup> C]Cimbi-36	[ <sup>11</sup> C]SB207145
Scan time (min)	90	120	90	120	120
Frame lengths (number x sec)	6x10, 3x20, 6x30, 5x60, 5x120, 8x300, 3x600	6x5, 10x15, 4x30, 5x120, 5x300, 8x600	6x10, 6x20, 6x60, 8x120, 19x300	6x10, 6x20, 6x60, 8x120, 19x300	6x5, 10x15, 4x30, 5x120, 5x300, 8x600
Realigned frames (first:last)	10:36	10:38	13:45	13:45	10:38
Reference frame	26	26	27	27	26

8